

Supporting information for

Chemical Reactions at the Graphitic Step-Edge: *Changes in Product Distribution of Catalytic Reactions as a Tool to Explore the Environment within Carbon Nanoreactors.*

Maria A. Lebedeva,^{a,b*} Thomas W. Chamberlain,^{a,c} Alice Thomas,^a Bradley E. Thomas,^a Craig T. Stoppiello,^a Evgeniya Volkova,^d Mikhail Suyetin,^d Andrei N. Khlobystov^{a,e}

^a School of Chemistry, University of Nottingham, University Park, Nottingham, NG7 2RD, UK.

^b Department of Materials, University of Oxford, 16 Parks Road, Oxford, OX1 3PH, UK.

^c School of Chemistry, University of Leeds, Leeds, LS2 9JT, UK.

^d Institute of Mechanics of Ural Branch of Russian Academy of Sciences, T. Baramzinoy St., 34, Izhevsk, 426067, Russian Federation.

^e Nottingham Nanotechnology and Nanoscience Centre, University of Nottingham, University Park, Nottingham, NG7 2RD, UK.

e-mail: maria.lebedeva@materials.ox.ac.uk

- 1. Catalyst preparation.**
- 2. Catalyst characterization.**
- 3. Catalytic studies.**
- 4. ¹H NMR spectra.**
- 5. Additional substrates investigated.**
- 6. Leaching tests under the catalytic conditions**
- 7. Recyclability studies**
- 8. Reaction mechanism**
- 9. Theoretical modelling**

Catalyst preparation.

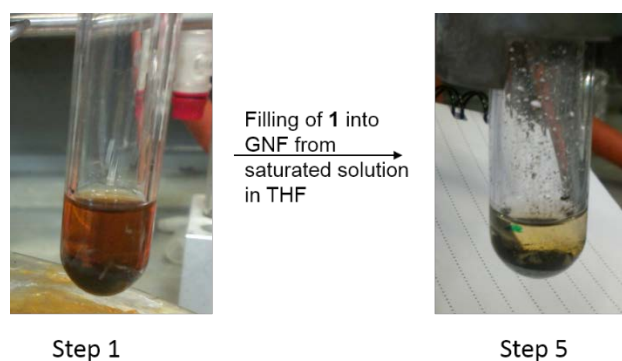


Figure S1. Solution filling of **1** into GNF from saturated THF solution showing a photo of the mixture after addition of GNF on the first iteration (left), and a photo of the same mixture after 5 consecutive solvent removal and refilling iterations. A gradual reduction in the colour of the solution is observed indicating encapsulation of the majority of molecules of **1** into the inner channel of the GNF.

1. Catalyst characterisation.

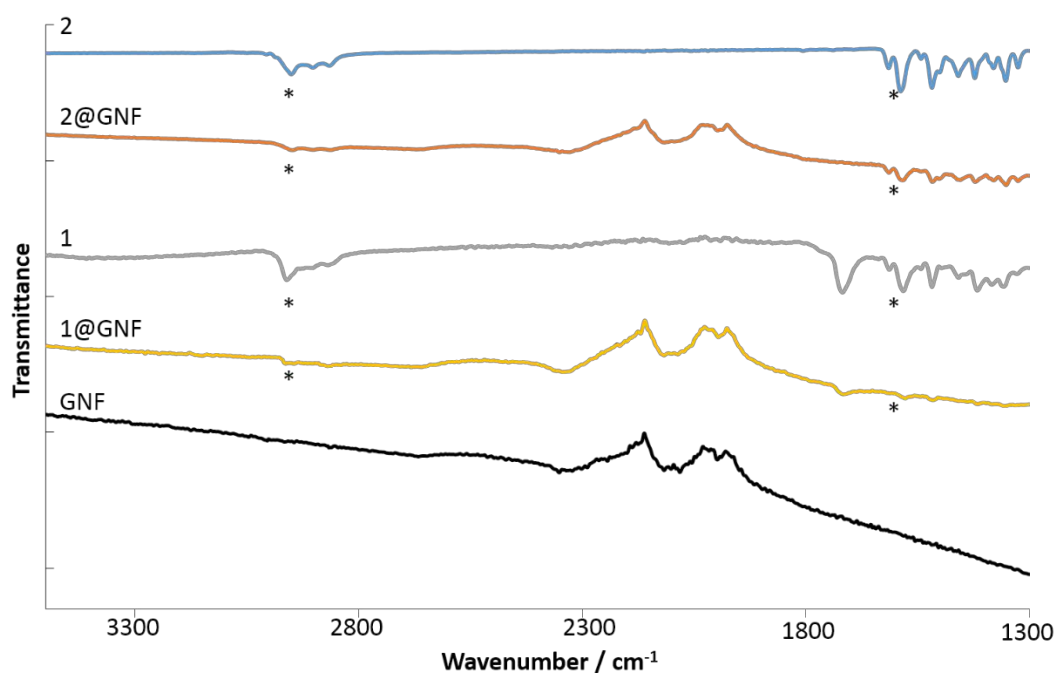
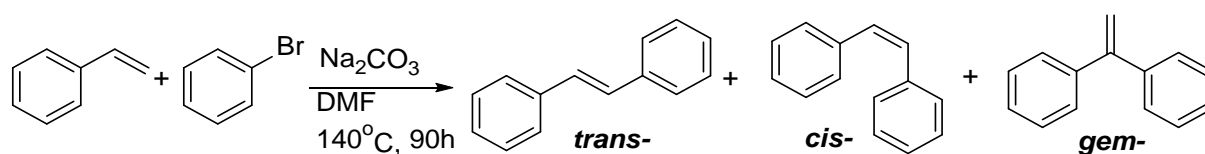


Figure S2. ATR FTIR spectra of **1**, **1**@GNF, **2**, **2**@GNF and GNF. The asterisk indicates the characteristic C-H bond stretches at $2800\text{--}3000\text{ cm}^{-1}$, and CH=N stretches of the salen fragments at 1615 cm^{-1} , in both molecular catalysts and the corresponding composite materials.

3. Catalytic studies.

Heck reaction parameters such as catalyst loading and reaction times were optimised in the model reaction between styrene and bromobenzene catalysed by **2** (Scheme S1). Catalyst loadings of 0.1 %, 0.5 % and 1 % were utilised, and samples were taken after 24 h, 65 h and 90 h to analyse by ^1H NMR (Table S1).



Scheme S1. Heck reaction between styrene and bromobenzene.

Table S1. Results of the Heck reaction between styrene and bromobenzene catalysed by **2** in different loadings over different time intervals.

Loading of 2	Reaction time, h	Conversion
-	90	0 %
-, GNF added	90	0 %
0.10%	24	3 %
	65	8 %
	90	11 %
0.50%	24	
	65	15 %
	90	18 %
1%	24	6 %
	65	28 %
	90	37 %

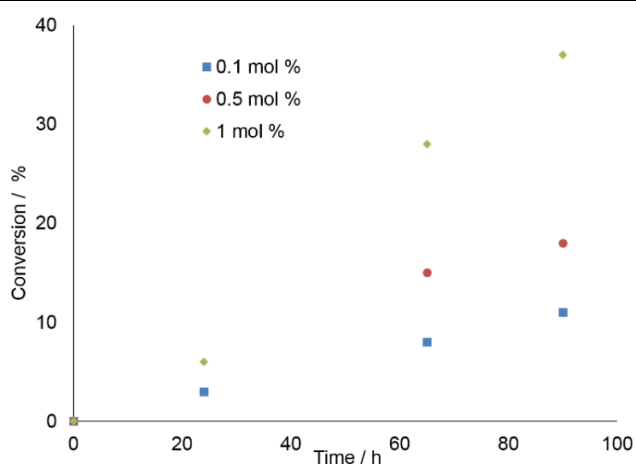


Figure S3. Kinetic curves of the reaction between styrene and bromobenzene catalysed by **2** in different loadings under homogeneous conditions.

4. ^1H NMR spectra.

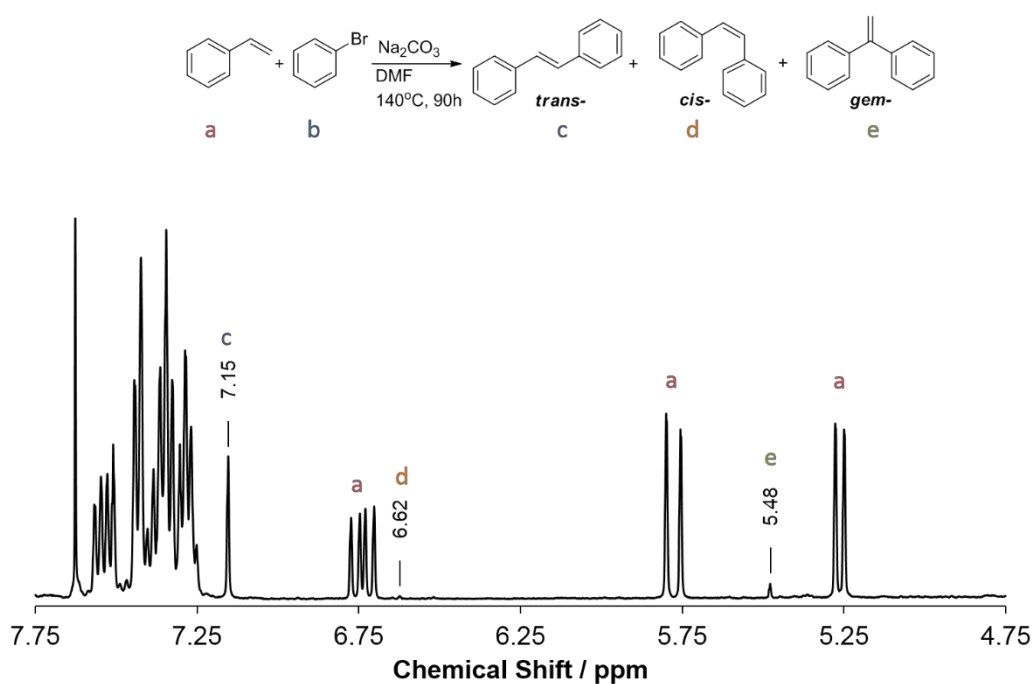


Figure S4. ^1H NMR spectrum of the reaction mixture between styrene (a) and bromobenzene (b) catalysed by Pd(II) catalyst after 90 h yielding *trans*- (c), *cis*- (d) and *gem*- (e) coupling products.

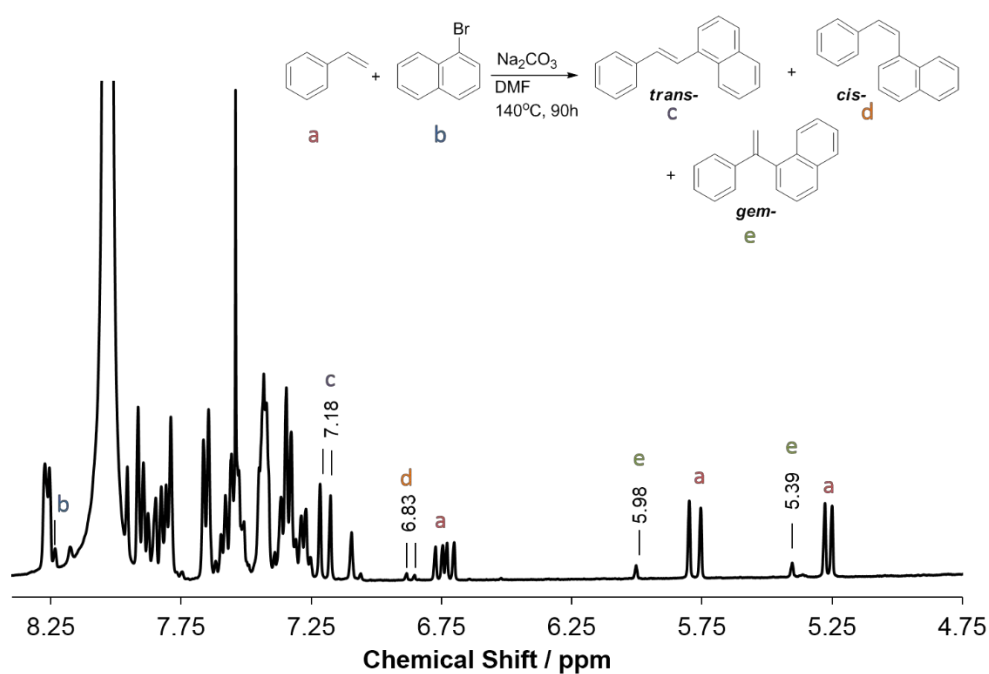


Figure S5. ^1H NMR spectrum of the reaction mixture between styrene (a) and 1-bromonaphthalene (b) catalysed by Pd(II) catalyst after 90 h yielding *trans*- (c), *cis*- (d) and *gem*- (e) coupling products.

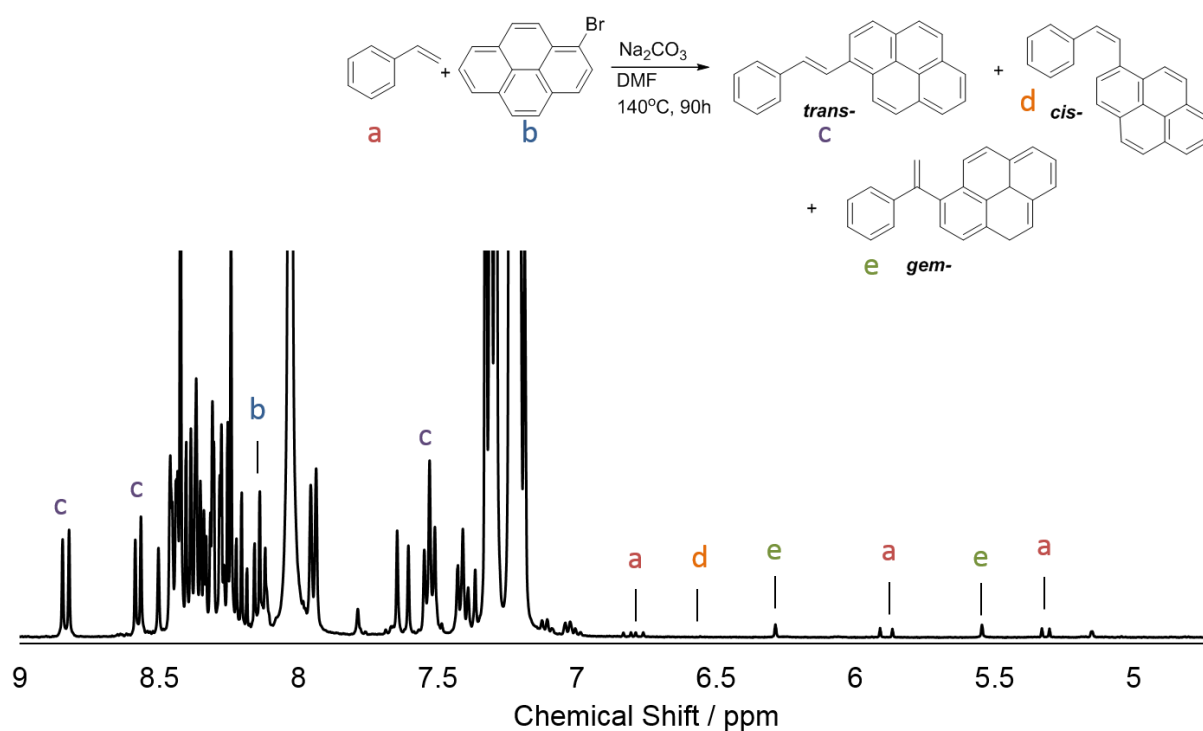


Figure S6. ^1H NMR spectrum of the reaction mixture between styrene (**a**) and 1-bromopyrene (**b**) catalysed by Pd(II) catalyst after 90 h yielding *trans*- (**c**), *cis*- (**d**) and *gem*- (**e**) coupling products

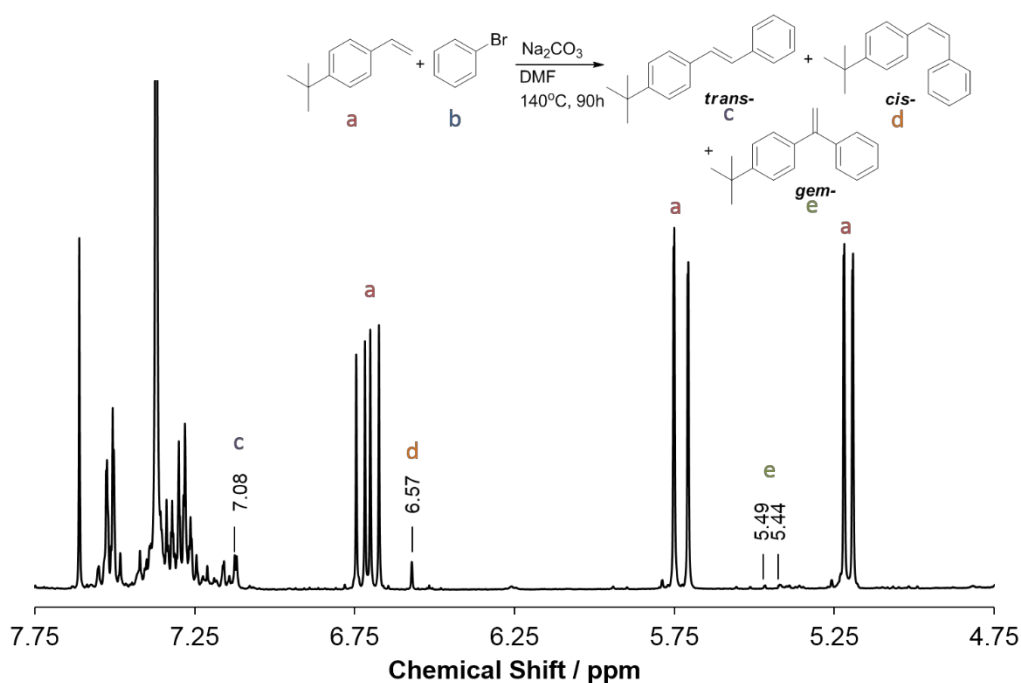


Figure S7. ^1H NMR spectrum of the reaction mixture between 4-*tert*-butyl styrene (**a**) and bromobenzene (**b**) catalysed by Pd(II) catalyst after 90 h yielding *trans*- (**c**), *cis*- (**d**) and *gem*- (**e**) coupling products.

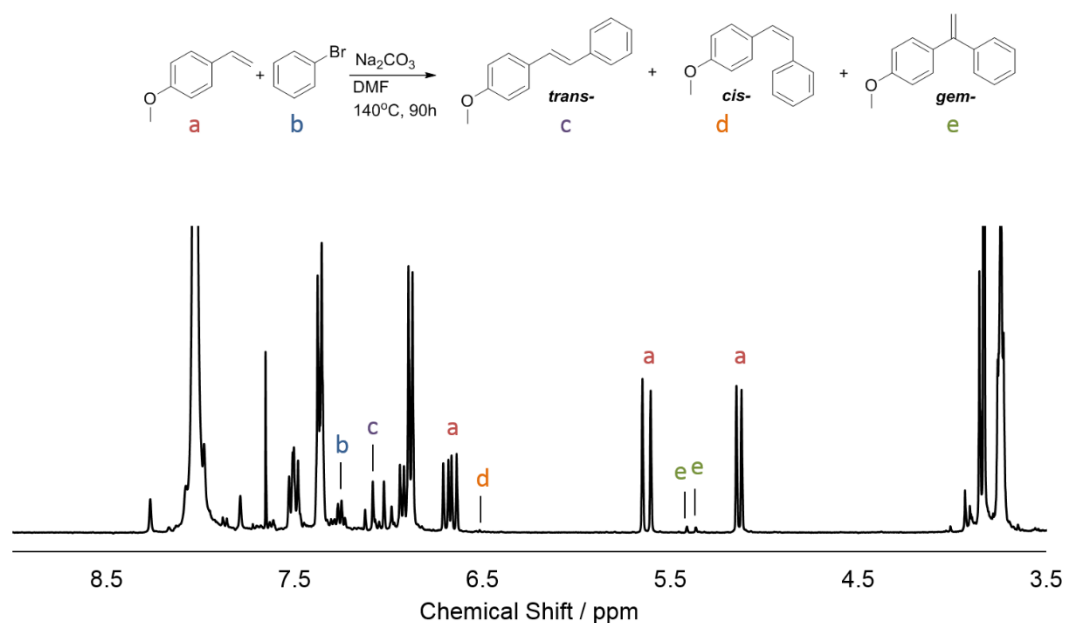
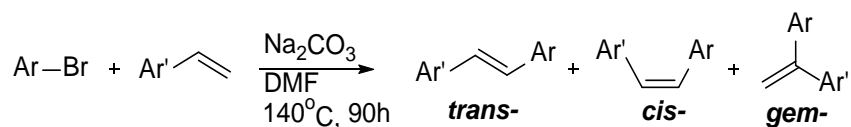


Figure S8. ^1H NMR spectrum of the reaction mixture between 4-methoxy styrene (**a**) and bromobenzene (**b**) catalysed by Pd(II) catalyst after 90 h yielding *trans*- (**c**), *cis*- (**d**) and *gem*- (**e**) coupling products.

5. Additional substrates investigated.



Scheme S2. Heck reaction between aryl bromide and aryl alkene.

Table S2. Conversion, TON/TOF and selectivities towards *trans*-, *cis*- and *gem*- coupling products in the Heck reaction between several other tested aryl alkenes and aryl bromides catalysed by **2** under homogeneous or heterogeneous conditions. All yields determined by ^1H NMR as averages of 3 experiments, with an experimental error of $\pm 2\%$.

Reagents	Catalyst	Conversion / %	TON ^a	TOF ^b	Selectivity / %		
					<i>trans</i>	<i>cis</i>	<i>gem</i>
	2	0	0	0	0	0	0
	2	9	18	0.20	86	6	8
	2	7	14	0.16	100	0	0
	2@GNF	9	18	0.20	100	0	0

reaction conditions: DMF, 140 °C, 90 h, 0.5 mol. % catalyst

^a TON determined as [mol product]/[mol catalyst]

^b TOF determined as [mol product]/([mol catalyst]*hour)

6. Leaching tests under the catalytic conditions.

The leaching experiments under catalytic conditions were performed to determine whether the catalyst molecules are retained on the GNF support during the catalytic process. The Heck reaction between styrene and bromobenzene catalysed by **1**, **1**+GNF, **1**@GNF, **2** and **2**@GNF was carried out under typical conditions (see experimental section for details). After 90 h the reaction mixture was filtered hot, and the filtrate was concentrated to remove the solvent. The residue was then redissolved in CHCl₃ (4 mL), and resulting solutions were analysed by UV/vis spectroscopy (Figure S5).

The resulting UV/vis spectra clearly show the absorption bands characteristic for **1** (524 nm) or **2** (497 nm) in each case. However comparison with the absorption spectra of pristine **1** and **2** also reveals the presence of broad featureless absorption bands over the whole visible range in the spectra of reaction mixtures (Figure S5 a,b) which are absent in the spectra of pristine complexes (Figure S5, c) and are most likely corresponding to the absorption of reaction products and/or starting materials. Therefore precise quantification of catalyst concentration in solution in each case is not possible by absorption spectroscopy only. However the relative ratios of absorption maxima at 524 nm for **1**, **1**+GNF and **1**@GNF allow to suggest that approximately 10 % of the molecules of **1** are leached in solution in case of **1**@GNF and approx. 50 % of the molecules are leached in solution in case of **1**+GNF after 90 h. Similarly, approx. 50 % of the molecules of **2** are leached from **2**@GNF after 90 h.

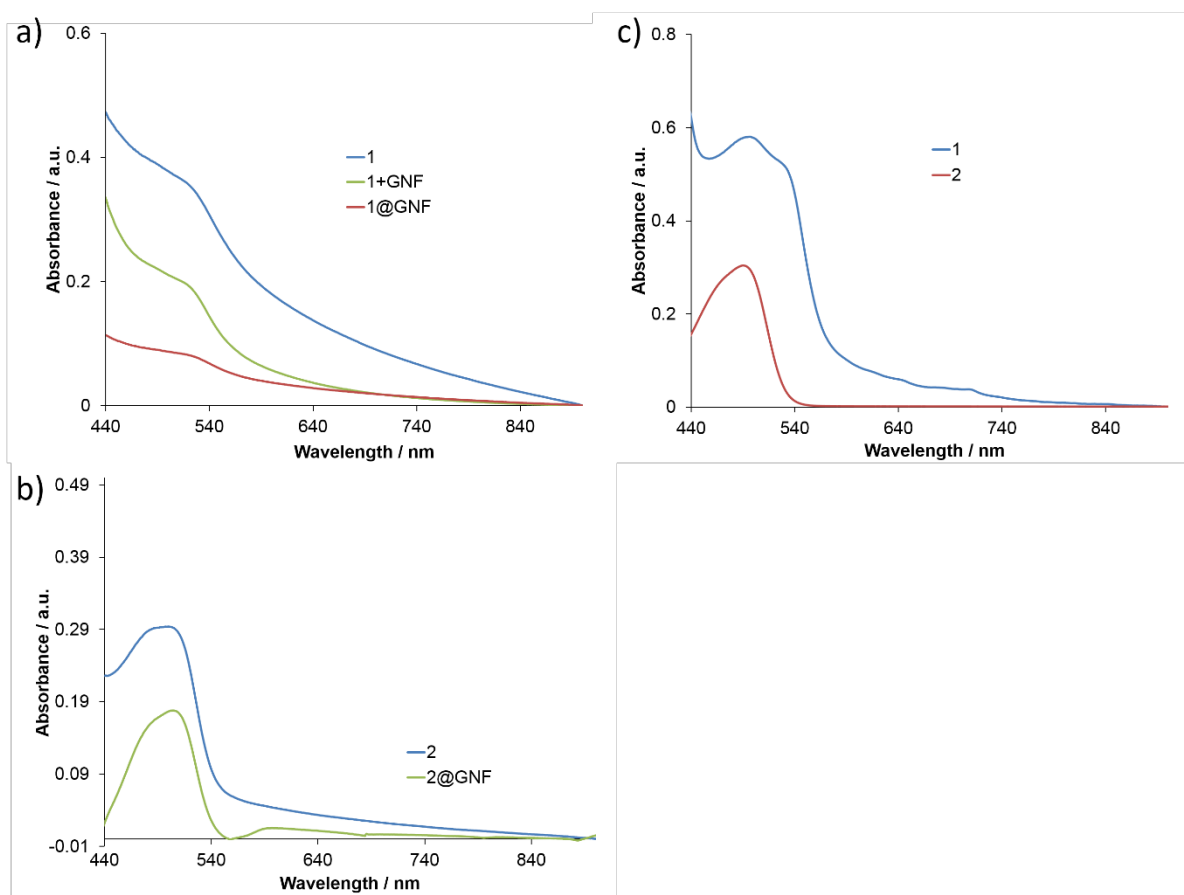


Figure S9. UV/vis spectra of Heck reaction mixtures catalysed by **1** (a) or **2** (b) obtained by the hot filtration of reaction mixtures after 90 h, removal of the solvent and dissolving in 4 mL of CHCl_3 indicating significantly lower concentrations of Pd catalyst for heterogeneous materials compared with the homogeneous reaction mixtures; and (c) UV/vis spectra of pristine **1** and **2** in CHCl_3 .

7. Recyclability studies.

The recyclability of **1@GNF** and **2@GNF** was investigated by utilising each heterogeneous catalyst in a series of consecutive catalytic cycles. The catalytic reaction between styrene and bromobenzene in the presence of each catalyst was carried out under identical conditions over 90 h, the catalyst was then separated by filtration, washed with an excess of CH_3CN , and employed in the next otherwise identical cycle. **1@GNF** maintains an activity of over 90 % after three consecutive cycles, before slowly deactivating due to gradual leaching of the molecules into solution over the cause of reaction and subsequent separation procedures. The activity of **2@GNF** drops sharply to less than 20 % of its initial value after the first cycle as a result of catalyst leaching during the separation and purification steps due to the lower affinity

of **2** to the step-edges of the GNF and higher solubility in polar CH₃CN utilised during catalyst recovery.

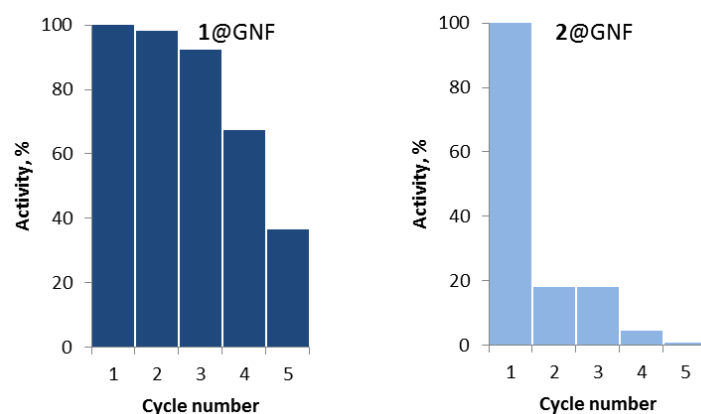


Figure S10. Comparison of the stability and recyclability of the catalyst in **1**@GNF (dark blue) and **2**@GNF (light blue) in five consecutive Heck reaction cycles of 90 h between styrene and bromobenzene.

8. Reaction mechanism.

The selectivity of the reaction towards *trans*-, *cis*- or *gem*- adducts is determined in several crucial steps of the catalytic cycle discussed below (Figure S11).

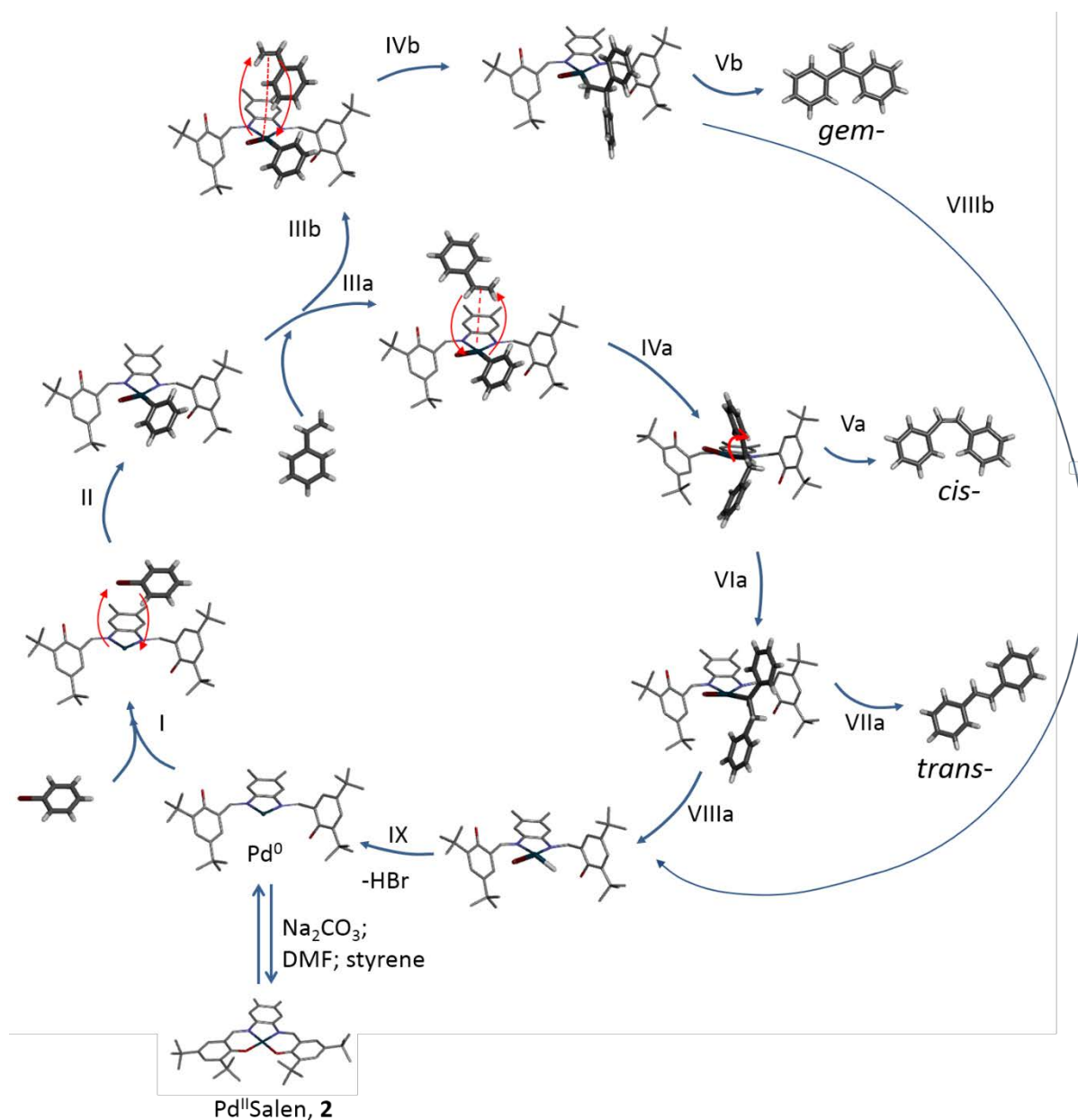


Figure S11. Proposed mechanism of the $\text{Pd}^{\text{II}}(\text{Salen})$ (**2**) catalysed Heck reaction which, initiated by the formation of the Pd^0 species, undergoes oxidative addition of bromobenzene (step I and II) followed by formation of a π -complex with the double bond of styrene (step III) in either vicinal (step IIIa) or geminal (step IIIb) orientations. The π -complex then undergoes alkene insertion (step IVa) followed by elimination yielding the *cis*-stilbene (step Va) or a C-C rotation (step VIa) followed by elimination yielding the *trans*-stilbene (step VIIa). The catalyst is then regenerated in steps VIIIa,b and IX by elimination of HBr. Carbon atoms are coloured in grey, hydrogen in white, oxygen in red, nitrogen in light blue, palladium in dark blue, bromine in dark red. N.B. The hydrogen atoms in ligand part of the catalyst molecule are omitted for clarity throughout.

In the initial step, the catalytically active Pd(0) species is generated via the *in situ* reduction of Pd(II)(Salen) with the solvent, the alkene or the base acting as a reducing agent.^[1] In the following steps, I and II, oxidative addition of bromobenzene to a Pd(0) centre takes place followed by the formation of a π -complex with the double bond of styrene (step III). Asymmetric alkenes can bind in two different orientations, with the regioselectivity guided by both electronic and steric factors, with the steric effects being dominant ^[2]. As a result the least sterically hindered orientation is preferred, (IIIa), resulting in the formation of the vicinal regioisomer. However binding in the more sterically hindered orientation can also take place (step IIIb), additionally stabilised by π - π stacking between the aromatic rings of bromobenzene and styrene, leading to the formation of the more sterically hindered geminal regioisomer. The resulting π -complex then undergoes *syn* insertion of the alkene (step IV) followed by a fast strain relieving C-C rotation (step VIa) and *syn* elimination (step VIIa) to give the most thermodynamically favourable product, the *trans*-alkene. However if this rotation is hindered, elimination can occur faster than the time taken for the rotation to take place. In such cases the kinetic *cis*-alkene is formed (step Va). The geminal coupling product is formed in a similar manner by *syn* elimination from the corresponding intermediate (step Vb). The catalyst is then regenerated by the reductive elimination of HBr in the presence of base in steps VIII and IX.

9. Theoretical modelling.

Before investigating the binding energy between the two sets of components in this study, i.e. **1** and GNF, and **2** and GNF, different force-fields (Universal Force Field (UFF) [3], Dreiding [4] and Compass [5]) were tested to calculate the binding energy of a well-known model system, fullerene C₆₀ encapsulated in a (10,10) single-walled carbon nanotube (SWNT).

Our simulations revealed that all of these commonly used force-fields dramatically overestimated the binding energy of the C₆₀@(10,10)SWNT system in comparison to available experimental and simulation data: -3.0 eV [6] as it is presented in Table S2.

L. Tang and X. Yang in [6] used new Lennard-Jones parameters for carbon atoms in order to correctly describe the encapsulation of C₆₀ in a (10,10) SWNT. We therefore implemented these parameters to the UFF used for all carbon atoms, leaving all other parameters like bond stretching, angle bending etc. unchanged. The modified force field is labelled; UFF_corrected. The calculated binding energy of C₆₀@(10,10) with the new force field applied is -2.87 eV and

it is much better agreement with experimental data [6]: the relative error obtained is very small - 4.33(3)%.

Table S3. Binding energy of C₆₀ encapsulated in a (10,10) SWNT calculated using different force-fields.

Force Field	Binding Energy: C ₆₀ @(10,10)/eV
Dreiding	-5.32
Compass	-8.97
UFF	-5.82
UFF_corrected	-2.87

Additional calculations showed that the binding energy of a single C₆₀ to graphene is -0.72 eV, which is close to the data reported in [7], where the binding energy of a single C₆₀ molecule to graphite is -0.85 eV.

Utilising the new force field - UFF_corrected, simulations to explore the binding between **1** and GNF, and **2** and GNF were performed using a molecular mechanics approach. Partial atomic charges of **1** and **2** were calculated using Qeq technique [8]. The size of the GNF is shown in Figure S12. Dangling bonds of GNF were saturated by hydrogen atoms. All atoms of GNF are neutral and frozen. The resulting binding energies are summarised in Table 2 of the main manuscript.

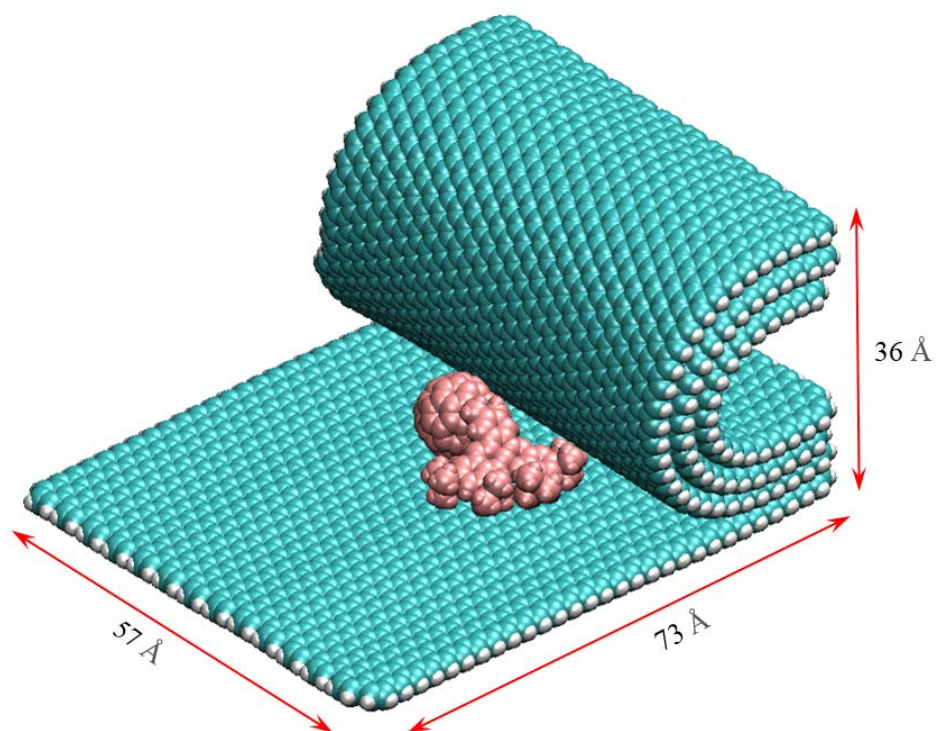


Figure S12. Modelling of **1** on the step edge of a GNF.

Additional simulations performed reveal that the binding energy of C_{60} to the step-edge of a GNF is -1.39 eV, which is two times larger than the binding energy of C_{60} to graphene indicating interactions with the two graphitic surfaces of the GNF step (Figure S13). The binding energy of **2** to graphene was also calculated using the same approach and was found to be -1.43 eV.

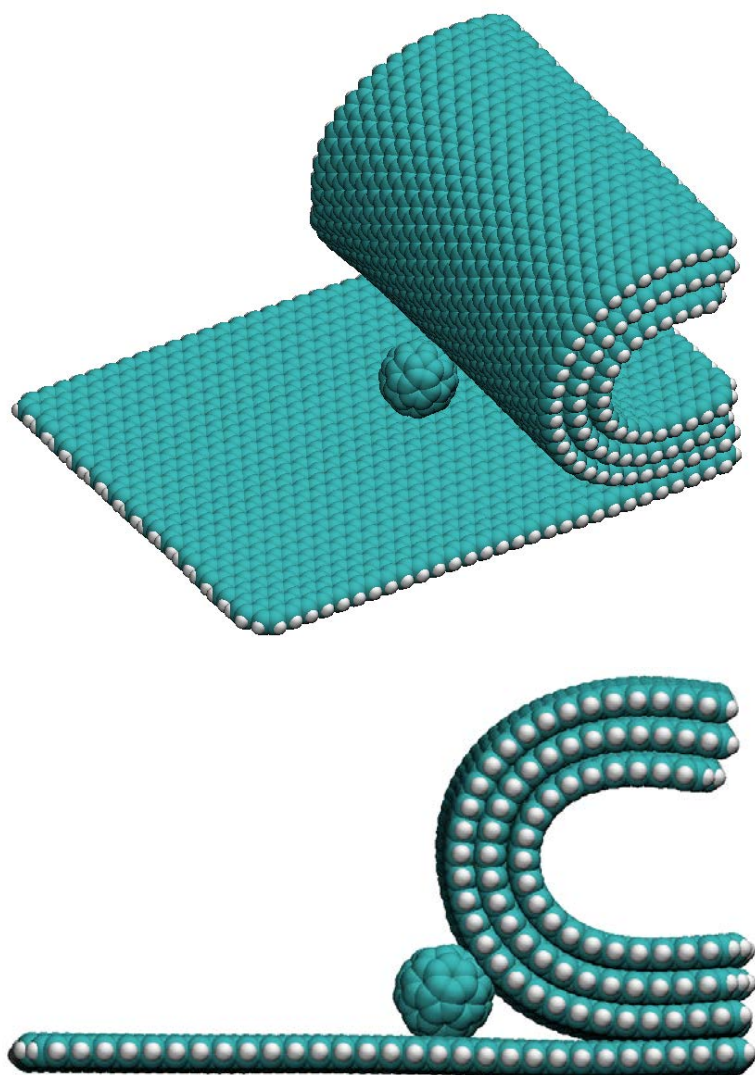


Figure S13. Absorption of pristine C₆₀ on the step-edge of a GNF.

References:

1. R.F. Heck, *J. Am. Chem. Soc.*, **1969**, *91*, 6707–6714.
2. (a) I.P. Beletskaya, A.V. Cheprakov, *Chem. Rev.* **2000**, *100*, 3009-3066; (b) A.M. Trzeciak, J.J. Zi'olkowski, *Coord. Chem. Rev.* **2005**, *249*, 2308–2322; (c) N. T. S. Phan, M. Van Der Sluys, C. W. Jones, *Adv. Synth. Catal.* **2006**, *348*, 609 – 679; (d) J. Ruan J. Xiao, *Acc. Chem. Res.* **2011**, *44*, 614–626.
3. A. Rappé, C. Casewit, K. Colwell, W. Goddard III, W. Skiff, *J.Am.Chem.Soc.* **1992**, *114*, 10024.
4. S. Mayo, B. Olafson, W. Goddard III, *J.Phys.Chem.* **1990**, *94*, 8897.
5. H. Sun, *J.Phys.Chem.B.* **1998**, *102*, 7338.
6. L. Tang and X. Yang, *J. Phys. Chem. C*, **2012**, *116*, 11783.
7. H. Ulbricht, G. Moos, T. Hertel. *PRL*, **2003**, *90*(9) 095501.
8. A.K. Rappe and W. A. Goddard, *J. Phys. Chem.*, **1991**, *95*, 335